Structural and Tribological Properties of Multicomponent Coatings on 45 and 210Cr12 Steels Obtained by Electrospark Deposition with WC-B$_4$C-TiB$_2$-Ni-Cr-Co-B-Si Electrodes

T. G. Penyashki[a], *, D. D. Radev[b], **, M. K. Kandeva[c], ***, and G. Kostadinov[a], ****

[a]*Institute of Soil Sciences, Agro-technologies and Plant Protection "Nicola Poushkarov", Sofia, 1331 Bulgaria*
[b]*Institute of General and Inorganic Chemistry-BAS, Sofia, 1113 Bulgaria*
[c]*Technical University, Sofia, 1000 Bulgaria*
*e-mail: tpeniashki@abv.bg
**e-mail: ddradev@gmail.com
***e-mail: kandevam@gmail.com
****e-mail: gdkostadinov@gmail.com

Abstract—In the present work, a new type of wear-resistant coatings obtained on steels by contactless electrospark deposition using a rotating electrode and by electrical discharge deposition with a vibrating electrode has been studied. Electrodes have been obtained by pressing and sintering multi-component powder mixtures of hard metal WC-Co with additives of super-hard and refractory compounds of B$_4$C and TiB$_2$ and semi-self-fluxing alloys Ni-Cr-B-Si. High density coatings, with a thickness up to 80 μm and micro hardness up to 17.0 GPa, have been obtained. The roughness, thickness, composition, and structure of the coatings thus obtained have been studied by X-ray diffraction, scanning electron microscopy, and electro-spark deposition. The influence of micro-geometric parameters, composition and structure of coatings on their tribological properties and wear resistance were studied by comparative tests of friction and abrasion wear. The friction tests showed that the wear of the coated steel surfaces is up to 5 times lower compared to the uncoated those. On the base of the experimental data, a comparative analysis of the coatings obtained by the two methods have been made. Appropriate regimes and conditions for deposition of coatings with optimal properties have been defined.

INTRODUCTION

A contemporary direction in the field of electrospark deposition (ESD) is the production of coatings with increasingly high hardness and wear resistance. In order to achieve an improved life of a coated surface, it is necessary to select an appropriate composition of electrode materials and process parameters for ESD. From practical and theoretical points of view [1—10], it is obvious that a further increase in the effect of ESD is related to obtaining coatings from harder and higher wear-resistant materials and, respectively, with better operational properties. It is also necessary to take into account the specifics of their behavior in the spark deposition process and to study the complex influence of the electrode materials on the properties and morphology of the coatings in parallel with the peculiarities of the methods and the electrical parameters of ESD.

In this connection, the objectives of the present work are to create new ESD coatings with higher hardness, wear resistance and tribological efficiency by using new electrode materials based on multi-component hard-alloy compounds and metals, to optimizing the quality characteristics, composition, and properties of the coatings obtained and to determine the ESD parameters for obtaining such coatings with increased properties compared to the existing ones. For those purposes, suitable materials have been selected and studied; a complex of the influences of the composition of the selected materials and process parameters of their deposition on the roughness, thickness, micro-hardness, composition, structure, and wear-resistance of the applied coatings was investigated.

Table 1. Chemical composition of substrate plates

Element, %	C	Cr	Si	Mn	Ni	Mo	W	Ti	Cu	V	P	S
210cr12 steel	1.9–2.2	11–12	0.1–0.4	0.15–0.45	Up to 0.35	Up to 0.2	Up to 0.2	Up to 0.03	Up to 0.3	Up to 0.15	Up to 0.03	Up to 0.03
45 steel	0.42–0.5	Up to 0.25	0.17–0.37	0.5–0.8	Up to 0.25	–	–	–	Up to 0.25	–	Up to 0.04	Up to 0.04

METHODOLOGY

Materials and Methods Materials, Equipment for ESD and Deposition Conditions

Substrate. Model plates of 45 carbon steel with hardness 190–210HB, and of 210cr12 heat treated steel with Rockwell C hardness 59–61, with sizes $10 \times 10 \times 4$ mm and polished to a roughness Ra = 0.63 μm, were used for substrate. The chemical composition of these steels is given in Table 1.

Implementation of ESD is ensured by rotary [6–10] or reciprocating (vibrating) movement of the layering electrode [1–5]. These are two different approaches requiring different regimes and equipment. The use of the first one requires special pulse generators and an electronic tracking system to maintain the gap between the electrode and the layered surface. The use of the second approach combined with a portable pulse generator and a hand-held electrovibrator provides complete versatility of the method and allows direct processing of large-dimensional details [1–5].

ESD is performed by a hand-held apparatus with vibrating movement of the electrode [1–5], (Fig. 1) and by contactless local electro-sprark deposition (LESD) (Fig. 2) [6–10]. In the vibration ESD, a "Carbide Hardedge" created by Aids Electronics Ltd is used with the following parameters: short circuit current—0.2–2 A; voltage—80 V; capacitance—5–

100 μF; oscillation frequency of the vibrator—100 Hz; and the single pulse energy was 0.03–0.3 J. In this work, the individual layering regimes with the single pulse energy $E_i = C.U^2/2 = 0.03-0.3$ J are numbered from 1 to 6 in order of an increase of the pulse energy (Table 2).

For LESD, a machine type "Elfa 541" with an increased pulse energy was used with the following parameters of the regime: current—$I = 1.6-32$ A; voltage—$U = 90$ V; capacitanceqQ$C = 0.22-5$ μF; pulse duration Ti = 3–20 μs; pulse fill factor $\tau = 0.1$; 0.2—(pulse frequency—5–66 kHz); single pulse energy $E_i = U.I. T_i = 0.005-0.05$ J; coating speed 0.5–1.0 mm/s. Number of passages of the electrode—$n = 1-4$. The rotation speed of the electrode was 1500 rpm.

Electrode Materials

Composite materials of B_4C, TiB_2, and WC were selected for the electrodes to provide both high wear resistance, such higher amount of transfer from the liquid phase and obtaining new additional wear-resistant compounds and phases in the process of forming the coatings. Boron carbide B_4C is a super hard mate-

Fig. 1. Device for manual electrical discharge deposition with vibrating electrode.
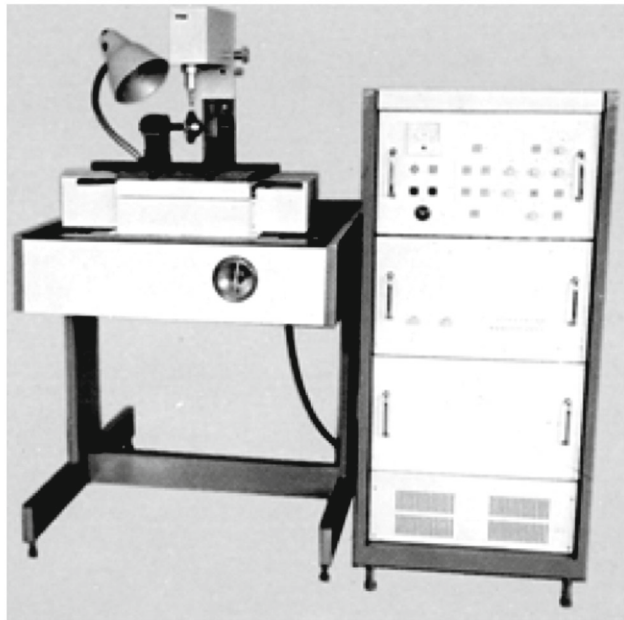

Fig. 2. Machine Elfa 541 for contactless LESD.

Table 2. Regimes for ESD with vibrating electrode

Regime	1	2	3	4	5	6
Capacitance, μF	5	10	15	20	50	100
Single pulse energy, J	$E_1 \approx 0.02$	$E_2 \approx 0.03$	$E_3 \approx 0.05$	$E_4 \approx 0.06$	$E_5 \approx 0.16$	$E_6 \approx 0.3$

**Table 3.** Chemical composition of the bonding powder mixtures

Element	C	Si	Cr	Fe	B	Ni
Percentage composition	0.61	2.86	12	3.94	3.6	Balance

rial with extremely high wear resistance and abrasion resistance but is brittle. The introduction of a less fragile and rigid components like titanium diboride—TiB_2 and tungsten carbide—WC, eliminates this problem. TiB_2 is distinguished by its very high hardness, wear resistance, and chemical resistance. According to published data, if compared with carbon, boride bonds are more difficult to decompose and it is expected for TiB_2 to be stored in a layer to a higher degree than those of WC and TiC. Both TiB_2 and WC, in addition to abrasive wear, are also resistant to impact loads.

Powders with chemical composition (see Table 3) are used as bonding phases of the above compounds.

The goal of the self-fluxing additives is to improve the ESD process and to obtain dense and uniform coatings with higher thickness and wear resistance [11−14]. The base powder "N_{base}" was prepared as a mixture of the bonding phase (Table 2) and WC in a ratio of 55:45 weight percentage. For the final electrode mixture with the additions of TiB_2, B_4C and WC, the conditionally designed "N" was adopted, which indicated that the bonding mixture is nickel-based. Carbide mixtures of WC + 8%Co − WK8 were added in order to increase the amount of WC and Co in the composition of the electrodes.

Two types of multi-component materials have been created with the following designations and composition:

$$- NW15B10T20 - 55\%N_{base} + 15\%WK8$$
$$+ 10\%B_4C + 20\%TiB_2;$$
$$- NW15T20 - 65\%N_{base} + 15\%WK8 + 20\%TiB_2.$$
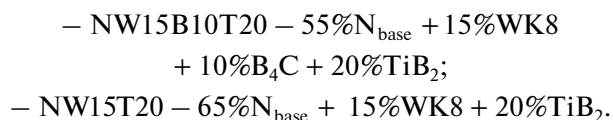
Initially, a milled and homogenized base mixture designed "N_{base}"—of 55% bonding metals (see Table 2) and 45% WC, was prepared. Next, the wear-resistant compounds B_4C, WK8, and TiB_2, in respective weight ratios, were added to the base mixture N_{base}.

Laminating electrodes with a diameter of 1−1.5 mm were obtained by electrically discharge cutting from monolithic plates prepared by the methods of powder metallurgy. Coatings of carbide composite electrode materials from 2.8% (Ta, Nb) C + 9%Co + WC and 16%TiC + 4.5% (Ta, Nb)C + 10.5%Co + WC, studied

and developed earlier [15, 16] and indicated WK9 and P25, respectively, were used as reference for comparison with the resulting coatings from the new electrodes.

Research Apparatus and Measurement Methodology

Balance WPS 180/C/2, which has 0.0001 g sensitivity, was used to determine the mass transfer, the increase of the weight of the cathode (mass gain of cathode)—Δk, mg, and anode material consumption—Δa, mg, at different process parameters for 1, 2, and 3 passes of an electrode. The mass transfer coefficient is given by the formula: $K = \Delta k/\Delta a$.

The surface roughness R_a, μm and thickness B, μm, of the resulting coatings were measured by profilometer AR-132B. Density, uniformity, and morphology of coatings were monitored by a VT-300 digital microscope.

The microstructure and microhardness—Vickers hardness (Hv), of the coatings have been studied by optical microscopy on cross-sectional and microhardness tests under indentation loads of 5 and 10 g by metallographic microscopes Neophot 22. Microhardness of the layer, of the sub-layer (in depth to the base), and of the base itself has been measured.

The phase identification, the distribution of elements in the surface layer and microstructural analysis of the coatings along with the interface region were performed with the support of an X-ray diffractometer Bruker D8 Advance in cobalt "Kά" and Cu radiation tube, an optical microscope, and an electron microscope "Bruker"; by scanning electron microscopy (SEM) and transmission electron microscopy.

The tribological properties and wear resistance of the coatings are investigated by comparative tests of friction with tribotester type "Thumb-disk" under dry surface friction with hard-fixed abrasive particles. The wear characteristics test method consists in measuring the mass wear "m" of the samples for a specific friction path "L" (friction cycles) under constant conditions—load "P" and glide speed "V".

The following wear characteristics were calculated:

− **Mass wear**—$m = m_0 - m_i$, mg

Table 4. Changes in anode mass loss and cathode gain for 1, 2, and 3 passages of the electrode at LESD on 45 steel

Electrode	No	Δa, g	Δa, g	Δa, g	$\Sigma\Delta a$, g	Δk, g	Δk, g	Δk, g	$\Sigma\Delta k$, g	$K = \Delta k/\Delta a$
		I pass.	II pass.	III pass.	For $n = 3$	I pass.	II pass.	III pass.	For $n = 3$	
WK9	1	0.0015	0.0012	0.0009	0.036	0.0011	0.0006	0.0005	0.0022	0.61
P25	2	0.0015	0.0009	0.0008	0.0032	0.0009	0.0005	0.0004	0.0019	0.59
NW15T20	4	0.0022	0.0019	0.0014	0.0055	0.0016	0.0012	0.0011	0.0039	0.71
NW150B10T20	5	0.002	0.0019	0.0014	0.0053	0.0014	0.0011	0.0010	0.0036	0.7

Table 5. Changes in anode mass loss and cathode gain at ESD on 45 steel

Rate, min/cm^2	2.5	5	7.5	2.5	5	7.5	–
Electrode	Δa, g	Δa, g	Δa, g	Δk, g	Δk, g	Δk, g	$K = \Delta k/\Delta a$
WK9	0.0031	0.0049	0.0059	0.0018	0.0028	0.0032	0.57
P25	0.0029	0.0046	0.0052	0.0016	0.0025	0.0029	0.54
NW15T20	0.0048	0.0069	0.0086	0.0030	0.0042	0.0053	0.61
NW15B10T20	0.0044	0.0061	0.0077	0.0024	0.0035	0.0044	0.57

— **Specific wear** (W_s): the ruptured mass of friction from the surface layer for normal load $P = 1 N$ per friction path $L = 1$ m and nominal contact area $Aa = 1$ mm^2: $W_s = \dfrac{m}{PL}$, mg/Nm

—**Wear intensity**—the amount of wear per unit of friction work: $W = \dfrac{m}{PL}$, where m is the wear of the solid for the test time, P—the normal load, L—the friction path passed.

—**Wear resistance** (W_r): Reciprocal value of the wear intensity.

RESULTS AND DISCUSSION

Coating Characterization—Roughness Ra and Thickness δ

When using contactless LESD, coatings have improved geometrical characteristics—higher density and uniformity, acceptable for the practical use repeatability, and lower roughness, which in most cases do not require further processing. Table 4 shows the gain of the cathode Δk, the mass loss of the anode material Δa and the transfer coefficient K obtained in contactless LESD with one, two, and three passes of the electrodes in regime $I = 14.4$ A; $C = 0.2$ μF; Ti = 12 μs; τ = 0.1, $V = 0.7$ mm/s.

Table 5 gives the data on the mass loss of the anode material Δa and the gain of the cathode Δk at ESD with a vibrating electrode on 45 steel. The coatings were performed in pulse energy 0.16 J—regime E_5 (see Table 2). As the mentioned Tables show, the peak efficiency is achieved with the NW15T20 and NW15B10T20 electrodes where the cathode growth is nearly twice as high compared to that obtained with

WK9 electrode Similar are the results obtained on 210cr12 substrate.

The results obtained show that at LESD with multi-component carbide alloys a transfer coefficient was achieved was achieved by 12–18% higher than that of the conventional tungsten carbides types WK9 and P25; the increment of the cathode $\Sigma\Delta k$ was up to 1.8 times higher than that of tungsten carbide electrodes. The cathode growth and the anode material consumption are well matched, and the mass of the cathode increases at a higher consumption of the anode material. With contactless LESD with new electrodes for 10 min/cm^2, the boundary of brittle destruction of the coating was not reached. From both Tables it is clear that at LESD the transfer coefficient K is up to 15–20% higher than at ESD with a vibrating electrode, but the values of Δa and Δk are significantly lower than those at the vibration ESD. Furthermore, the cathode growth in the vibration ESD with NW15T20 electrode is higher than that obtained with NW15B10T20 electrode, which is apparently due to the presence of B$_4$C which is not conductive. It seems B$_4$C reduces the toughness of the grain boundaries and a substantial part of the transferred anode material is in a fragile (softened) phase and does not adhere to the surface of the cathode.

The minimum and maximum values (borders) of the thickness δ, of the surface roughness Ra, and the microhardness Hv of coatings obtained from the studied electrodes at the different used values of parameters of regimens for ESD are all shown in Table 6.

From the data presented in Table 6 it is evident that the roughness values Ra are significantly lower than those obtained with the vibrating apparatus (Table 7) and the thickness δ is also lower. Table 7 presents data

Table 6. Range of changes of thickness, roughness, and hardness of deposited and tested coatings on 210cr12 and 45 steels obtained in selected regimes and electrodes via LESD

Electrode	Coatings on 210cr12 ($E_i = 0.001-0.03$J)				Coatings on 45 steel ($E_i = 0.001-0.03$J)			
	Ra, μm	δ, μm	Hv, GPa	Coeff. of hardening	Ra, μm	δ, μm	Hv, GPa	Coeff. of hardening
WK9	0.95–2.5	4.5–14	11–14	1.2–1.65	1.0–2.65	4–14	6–11	2.6–5
P25	0.9–2.2	4–12	11–16	1.2–1.65	1.0–2.65	4–14	6–12	2.6–5.4
NW15T20	1.3–3.6	3.5–20	12–15	1.4–1.75	1.3–3.5	4–18	7–12	3–5.4
NW15B10T20	1.3–3.5	3.5–18	12–16	1.4–1.85	1.35–3.7	4–16	7–14	3–6.3
Substrate 210cr12/45 steel	0.63	–	8.6	1.0	0.63	–	2.1	1.0

Table 7. Parameters of coatings obtained via ESD with vibrating apparatus on 210cr12 steel, $E_i = 0.03-0.3$J

No.	Electrode	Ra, mm	δ, mm	Hv, GPa	Coeff. of hardening
1	WK9	1.8–4.5	16–52	11–15	1.2–1.7
2	P25	1.8–4.2	13–40	11–16	1.2–1.9
3	NW15T20	2.5–6.5	20–90	12–15	1.4–1.7
4	NW15B10T20	2.5–6.5	20–80	12–17	1.4–2

on the thickness, hardness, and roughness of coatings at vibration ESD on 210cr12 steel.

The obtained results of vibration ESD show that an increase of the energy of the pulses (in the direction from regime 3 to regime 6—Table 2) leads to an increase in the thickness of the obtained coatings and to a significant increase of roughness and unevenness. The maximum thickness at which a relatively uniform coating with surface roughness up to Ra = 3–4 μm is obtained is in a range of 45–50 μm at regime 5, with pulse energy $E_5 = 0.16$J. Similar are the values of roughness and thickness of coatings applied to the upper electrodes onto 45 steel.

The results obtained at ESD on both steels demonstrate that at a higher amount of bonding metals in the composition of NW15T20 electrode, the thickness of the coatings is also higher. Therefore, an increase in the amount of bonding metals in the electrode material composition allows formation of coatings with a greater thickness. Figure 3a, 3b show the changes of surface roughness Ra and of thickness δ of LESD coatings onto 45 steel (depending on capacitance C).

Similar are the changes of Ra and δ depending on current I and pulse duration T_i, as well as those under the impact of electrical parameters on coatings applied on 210cr12 steel. The roughness and thickness of the coatings deposited on the two tested steels under
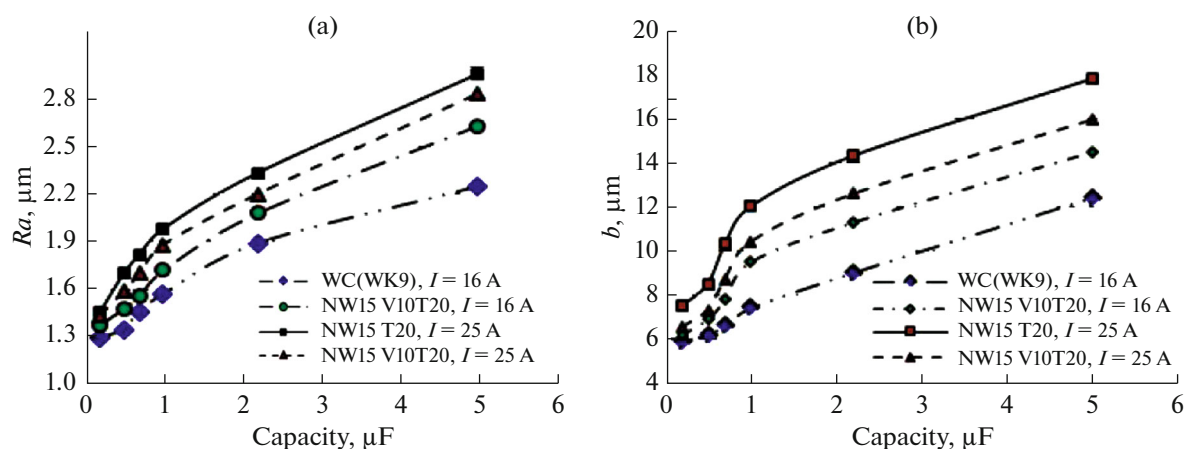
Fig. 3. Changes of *Ra* and δ of coatings in function of capacitance C in LESD-I = 22 A, Ti = 12 μs, U = 90 V, τ = 0.1, V = 0.6 mm/s, n = 2, on 45 steel substrate: (a) $Ra = f(C)$; (b) $δ = f(C)$.
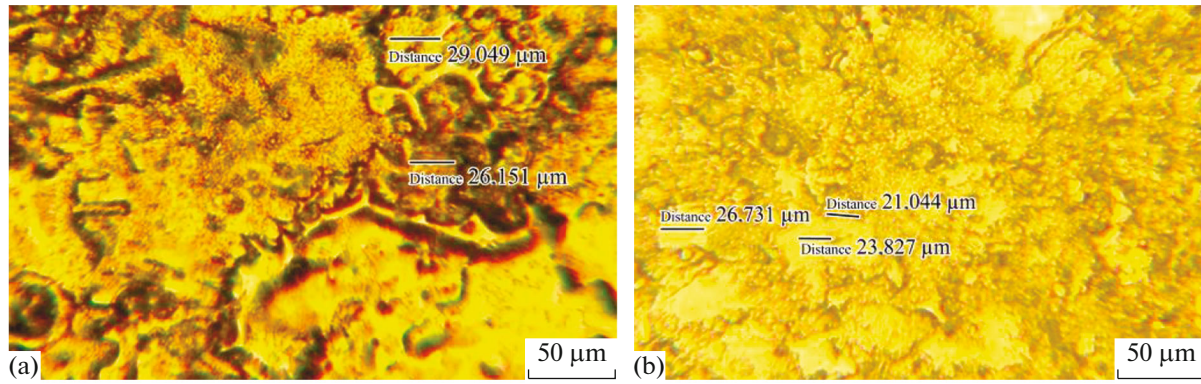
Fig. 4. Microphotography of coating surface obtained on NW15B10T20 electrode on 45 steel: (a) via vibration ESD, $E_i = 0.061$J; (b) via LESD, regime $I = 25$A, $C = 5$ μF, Ti = 12 μs, $\tau = 0.1$, 4 passes $E_i = 0.03$J.
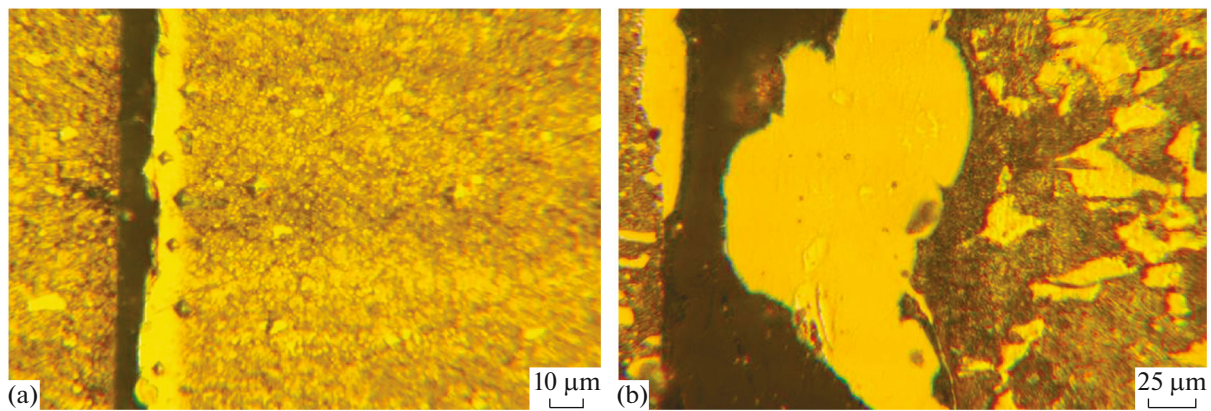

Fig. 5. Cross section images of coatings on: (a) NW10B10T20 electrode on 291cr12 steel, $E_i \approx 0.02$J, via contactless ESD; (b) on NW15B10T20 electrode on 45 steel, via continuous vibrational ESD, for 2 min, at the same point $E_i \approx 0.3$J.

somewhat different conditions do not vary significantly and increase with an increase in the energy of the pulses (Fig. 3). Their specific values are up to 30% higher than those obtained under the same conditions with WK9 electrodes (Fig. 3). Furthermore, the use of the new electrodes allows the rate of application to increase from 0.7 to 1mm/s without affecting the thickness of the coating. A higher thickness of the coatings can be explained by the presence of bonding metals forming an unlimited solid solution with the base material and by the presence of boron and silicon, which slows down the formation of oxide films and has a positive effect on the continuity and the increase of the thickness of the coating. In addition, the introduction of boron reduces the erosion resistance of the alloying electrode, as a result of which the transport of the electrode material to the surface to be processed increases [12–14].

Figure 4 shows the microphotography of coatings applied by vibration and contactless ESD on 45 steel.

The images of the microstructures obtained on the surface of the composite coatings indicate the formation of a coating from a melt. Carbide grains and the sections with a structure similar to amorphous are observables and distinguishable. Comparison of the surface of the coatings obtained by both methods shows that in LESD the coatings have smaller structural components, with no visible cracks and pores, while at vibrational ESD separate protuberances are seen with dimensions to 60 μm resulting from the fragile destruction of the electrodes.

Structure and Micro-Hardness of Coatings

The microstructure of the samples of the studied coatings has been revealed by using cross-section images and applying an optical microscope. Figure 5 presents the microstructures of some of the studied coatings.

As can be seen from Fig. 5a, the resulting coatings have a compact and uniform microstructure—a white layer with a low porosity that does not mix with the substrate. In LESD, a single smooth flat dense layer with a uniform thickness of up to 15 μm firmly

Table 8. Phase composition of coatings applied by LESD ($I = 25A$, $C = 2.2\ \mu F$, $T_i = 12\ \mu s$, $\tau = 0.1$, $n = 2$

Electrode	45 steel	210cr12 steel
	Phase composition	
WK9	$Fe\alpha$, $Fe\gamma$, W_2C, Fe_3W_3C, Fe_2W	$Fe\alpha$, $Fe\gamma$, Fe_3W_3C, W_2C, $(CrFe)_7C_3$, Fe_3C, Cr_3C_2, Fe_2W, Fe_2O_3, Fe_3O_4
P25	$Fe\alpha$, $Fe\gamma$, W_2C, Fe_2W, Fe_3W_3C, Fe_3C, $(TiW)C_{1-x}$ Fe_3O_4	$Fe\alpha$, $Fe\gamma$, Fe_3W_3C, Fe_2W, Fe_7W_6, W_2C, Co_3W_3C, Fe_3C, $(Ti,W)C_{1-x}$, Fe_2Ti, $(CrFe)_7C_3$, Fe_2O_3, Fe_3O_4
NW15T20	Fe,Cr_7C_3, TiB_2, Cr_3B_4, Cr-Ni-Fe-C.	$Fe\alpha$, $Fe\gamma$, Cr-Ni-Fe-C, WC_{1-x}, Cr_7C_3, Ti_2Fe, Fe_3C, Cr_3B_4, TiB_2, TiB, $FeNi_3$, traces of CrNiW, Fe_3W_3C, CrFe
NW15B10T20	Fe, Cr-Ni-Fe-C, Cr_7C_3, Cr, TiB_2, Cr_3B_4, B_4C, Cr_3B_4,	$Fe\alpha$, $Fe\gamma$, Cr-Ni-Fe-C, Cr_7C_3, WC_{1-x}, $Ti2Fe$, Fe_3C, Cr_3B_4,TiB_2, TiB, traces of $FeNi_3$, CrNiW, Fe_3W_3C, CrFe
Substrate	$Fe\alpha$, $Fe\gamma$	$Fe\alpha$, $Fe\gamma$, $(Cr, Fe)_7C_3$, Fe_3C, Cr_3C_2

Table 9. Phase composition of coatings applied by vibration ESD $- E_5 = 0.16J$ (reg. 5, Table 2)

Electrode	210cr12 steel
	Registered phases in the coating composition
WK9	$Fe\alpha$, $Fe\gamma$, Cr_7C_3, WC_{1-x}, Fe_3W_3C, traces of Fe_2O_3, Fe_3O_4, Fe-Cr, $(Cr, Fe)_7C_3$, Co_3W_3C
NW15T20	$Fe\alpha$, $Fe\gamma$, Cr_7C_3,WB_2, WB, $TiCo_3$,TiB_2, traces of W_2C, Fe_2B, CoB, CrFe, $FeNi_3$, CrNiW, Fe_3W_3C
NW15B10T20	WC_{1-x}, Fe, Cr_7C_3, Fe_2C, Cr_3B_4, TiB_2, Cr-Ni-Fe-C, traces of Fe_2B, CoB, B_4C, $FeNi_3$, CrNiW, CrFe, Fe_3W_3C
Sulstrate	$Fe\alpha$, $Fe\gamma$, Cr_7C_3, Fe_3C

attached to the substrate without visible microcracks and gaps is visible. In vibration ESD, the surface layer has a more uneven thickness. In all investigated coatings, the hardness of the white layer is higher than that of the substrate and varies too widely (Tables 6 and 7). However, the microhardness of coatings applied by vibration ESD with new electrodes is up to $10-15\%$ higher than that of LESD and than that obtained with WK9 electrodes. The highest values of Hv to 17 GPa were obtained at coatings from NW15B10T20 electrode in ESD on 210cr12 steel, however, the highest coefficient of an increase in the hardness after ESD was observed in the unhardened 45 steel—$K = 3.8–6$ times increase in Hv, while for hardened 210Cr12 tool steel, the coefficient was $1.4–2$. This indicates that the method and the new electrodes are more effective for application to unhardened carbon steels. From the parameters of the layering regime, at LESD, the most significant influence on the micro hardness of the coatings Hv is this of the duration of pulses T_i and capacitance C.

Phase Composition of Coatings

The main phases in the composition of the coatings are given in Tables 8 and 9. They are arranged sequentially in the intensity of the characteristic lines. The phase composition of WK9 and P25 electrodes coatings is provided as the base for comparison.

At ESD, the following main phases in the composition of the coatings on 210cr12 steel are registered: martensite (a-Fe) and a modified complex multi-component matrix of alloyed austenite (g-Fe)—Cr-Ni-Fe-C.

Modified carbides of the type WC_{1-x}, Cr_3B_4, TiB_2, and carbides of the basic material $(Cr Fe)_7C_3$, Cr_3C_2, Fe_3C are registered in small quantities (with a low intensity of peaks). Traces of Cr_2N, Fe_2N, Co_3W_3C and of metalloid compounds of Fe with W, Ti, and Cr are observed [17].

Besides the modified carbides and borides of the electrode material and the substrate, the coatings and new carbides and borides appear in the process of formation, obtained by the reaction between the bonding metals of the electrode and those of the substrate with boron and carbon.

Figure 6 shows X-ray diffraction (XRD) patterns of coatings deposited by vibration ESD with NW15T20 electrode on 210cr12 steel at regime 4-Ee = 0.06J, and by LESD with NW15B10T20 electrode on 45 steel at regime $I = 25$ A; $C = 0,2\ \mu F$, Ti = 12 μs, τ = 0,1, 2 passages $- E_2 = 0.03J$. XRD patterns differ both in the intensity and width of the characteristic lines of the characteristic lines of austenite and carbides and in the phase compo-sition. At ESD with NW15B10T20 electrode, in addition to the phases observed in coatings from NW15T20 electrode, the presence of a high wear-resistant phase B_4C is also registered. This indicates that boron carbide has partially retained its orig-
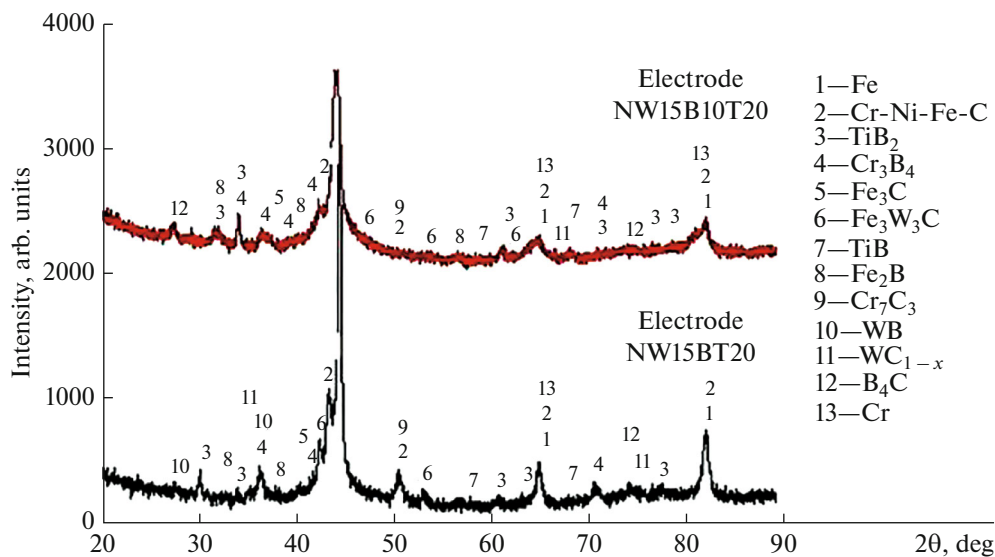
Fig. 6. XRD patterns of multi-component coatings deposited by LESD on 45 steel, with NW15B10T20 electrode, and by vibrational ESD on 210cr12 steel, with NW15T20 electrode.

inal form during the transfer process, while the free boron and boron from the titanium diboride, in which partial dissociation occurred combined with chromium and tungsten to form high wear resistant chromium and tungsten borides.

The characteristic diffraction peaks of the substrate (α-Fe, γ-Fe) are broadened and displaced, which reflects both the formation of solid solutions and the introduction of carbides and new compounds in the gamma iron, as well as grain refining of the structure to reaching to a structure less condition [18, 19]. The obtained results of XRD analysis show that the white layer is a mixture of disequilibrium heterogeneous finely grained martensitic-austenitic structure, saturated with modified ultra-disperse anodic carbides and borides, solid solutions, intermetallic compounds, and amorphous phases, whose part increases with an increase of energy for layering. The type and number of the phases constituting the white layer is determined by the type of the anode and cathode materials and by the ratios between them — by the energy for the processing.

The surface layers obtained via LESD have a lower content of components of the electrode material. The top layer is a mixture of the materials of the electrode and the substrate with a predominant content of the modified cathode material. The coating is uniform, with less roughness, but the content of the electrode material is lower than that obtained through vibration ESD.

At vibration ESD with the electrodes studied, the intensity of characteristic carbide and boride peaks is higher, therefore their quantity is also higher, which implies a higher wear resistance, but coatings are uneven, with high roughness, which makes them not suitable for tools with thin and sharp cutting edges.

From the XRD data for the coatings deposited on the investigated steels, it is found that their phase compositions are enriched with more carbides and borides than the conventional carbide electrodes. The multicomponent matrix of alloyed austenite—Cr-Ni-Fe-C and intermetallic compounds and the presence of ultra-dispersed different borides and carbides create preconditions for exceptional and unique qualities of the resulting coatings. Both NW15T20 and NW15B10T20 electrodes are emerging as promising materials for high-wear-resistant and multifunctional coatings.

Scanning Electron Microscopy Analysis of Coatings with New Electrodes

The following Figures show some of the results obtained by SEM analysis—the microstructure of the surface and the distribution of the elements in coatings deposited by NW15B10T20 and NW15T20 electrodes via vibration ESD on both steels.

Figure 7 shows the microstructure and distribution of elements on the coating surface from NW10B10T20 electrode deposited on 45 steel by vibration ESD (regime 6, Table 2, $E_6 = 0.3J$).

The elemental composition of the same coating is shown in Fig. 8.

The elemental composition in the glass-like coating area of NW15T20 electrode on 210cr12 steel in regime 4—($E_4 = 0.06J$) is shown in Figure 9. From Figs. 7–9, it can be seen that the micro relief of the obtained coatings is uneven and hetero-geneous both in structure as well as in composition. There is a diffusion of particulate of the electrode material in the cathode but also reverse diffusion of iron in the direction of the coating was observed.
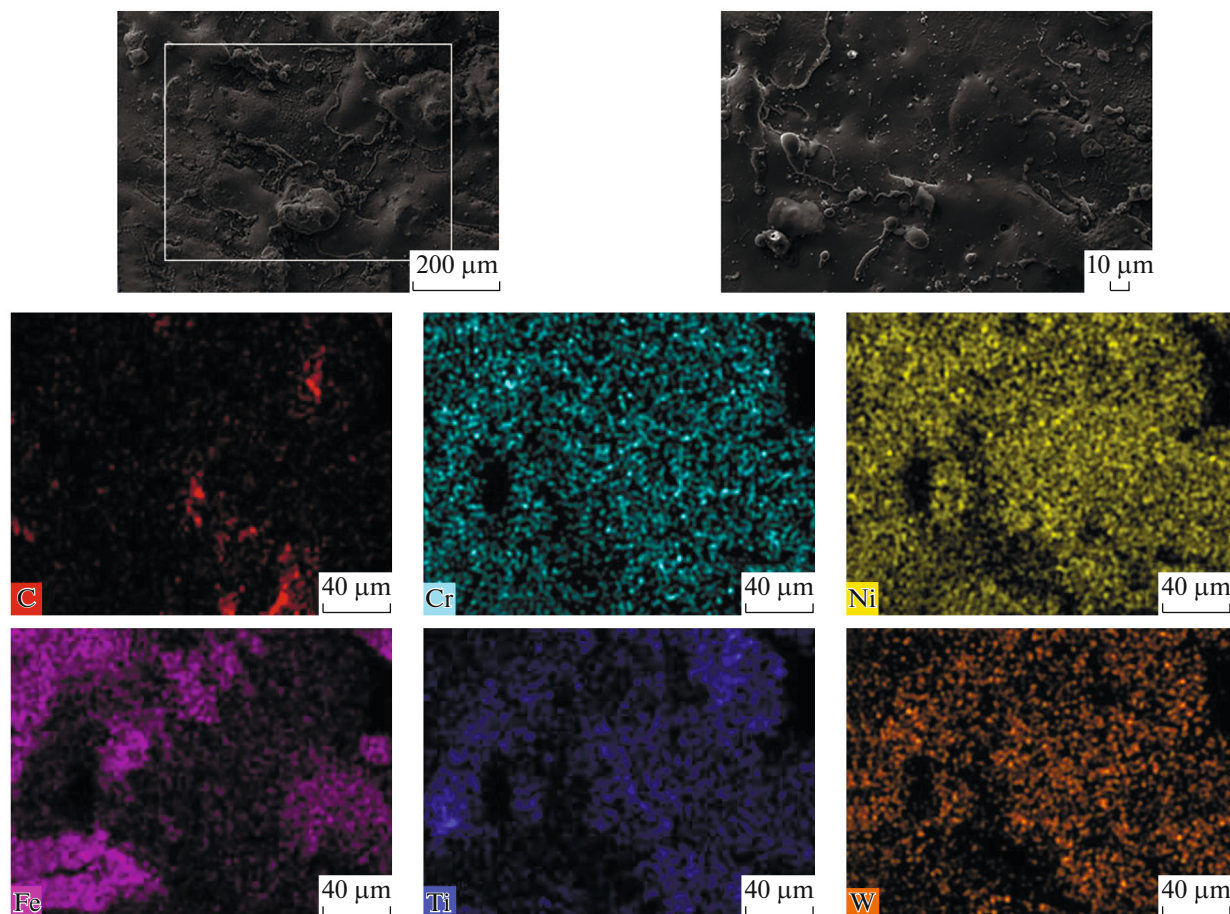
Fig. 7. Micro relief and distribution of elements in the coatings of NW15B10T20 electrode applied on 45 steel by vibration ESD, in regime 6 ($E_6 = 0.3$J).
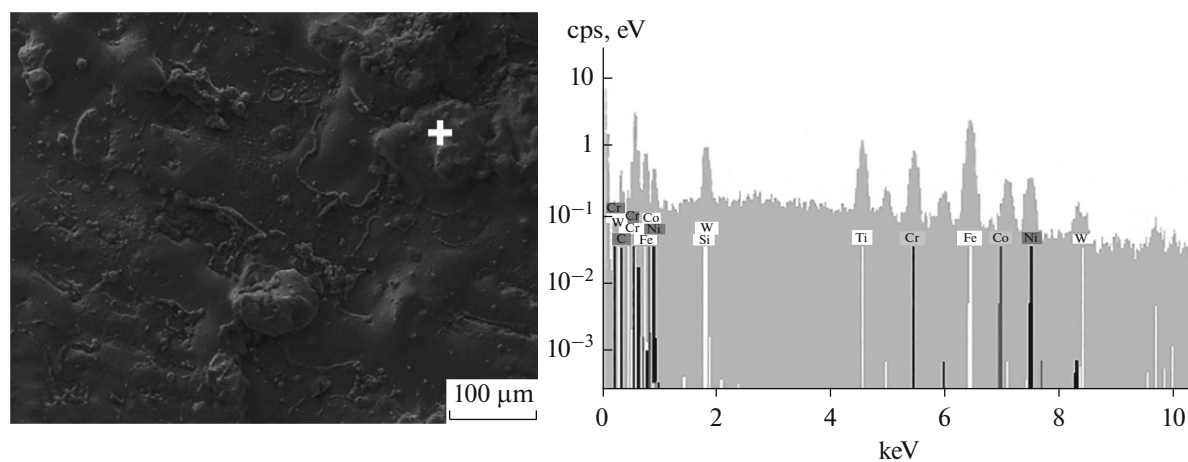

Fig. 8. Micro relief and elemental composition of the coating of NW10B10T20 electrode on 45 steel by vibration ESD, in regime 6 ($E_6 = 0.3$J).

The chemical composition of the coating differs significantly from the chemical composition of the electrode material. The quantitative microanalysis of the coatings detects the presence of Fe, Cr, Ni, Co, Si, B, C, Ti, and W. The light elements in the electrode material (C and B) partially burn or form new com-
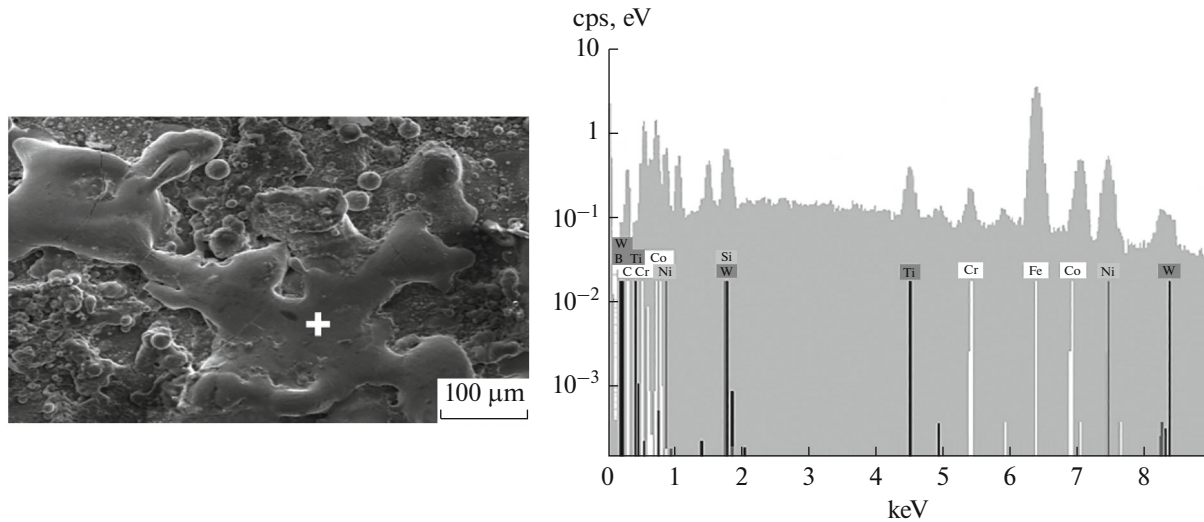
Fig. 9. Micro relief and elemental composition in the glass-like coating area of NW15T20 electrode on 45 steel by vibrational ESD, in regime 4 ($E_4 = 0.06$J).

pounds with the elements from the substrate and the electrode material. The distribution of Ti and W repeats that of C and B, which confirms that Ti and W are present in a bonded form in the form of carbides and borides.

Based on the data obtained, it can be concluded that the elements, that are not involved in the formation of carbides and borides, form a solid solution with iron. The formation of a metal matrix in the form of a solid solution is confirmed by the distribution of Ni, Cr, and Fe. In the course of the study, it was found that the distribution of Ni and Cr repeats the distribution of Fe, indicating that those elements form a solid solution. Judging by the distribution of Fe and Ti, it can be assumed that the latter element is mainly in the form of borides. Titanium diboride introduces some changes in the structure of the applied layer.

In the metallographic study of a cathode material, after a few minute of ESD, at the same point with NW15B10T20 electrode containing 20% TiB_2, several layers were noticed which follow one another and dif-

fer significantly in their structure from the sample material (Fig. 5b).

The micro hardness of the coatings is 6−17 GPa. However, there are separate measured values up to 19.5 GPa. The initial hardness of the ultra-hard compounds B_4C, TiB_2, and WC is 34, 33, and 25 GPa, respectively.

Lower values of microhardness of the coatings obtained with these materials can be accounted for by the change of their initial chemical composition, partial burning of carbon and boron in the transfer process, dissociation of those compounds and formation of new ones (Tables 5 and 6) and also by the presence of iron from the substrate in the coating composition as shown by the results of the analyses performed.

Wear Resistance of Coatings Obtained

Tables 10, 11, and Fig. 10 give the results of the comparative experimental studies of the influence of the materials and the ESD regimes on the tribo-technical properties of the resulting coatings.

From the results, it was established that the coated samples have 2−5.8 times lower wear than uncoated ones and up to 1.5 times lower than the deposited samples with WK9 electrode. Similar are the changes in the wear rate, wear intensity, and wear resistance of coatings (Table 11). The lowest wear at ESD with NW15B10T20 electrode was obtained in the pulse energy regime $E_i = 0.05−0.06$ J, while at NW15T20 electrode—at $E_6 = 0.3$ J.

These coatings reduce the wear intensity stronger than coatings of conventional tungsten hard alloys, slowdown wear development over time, and can be used to increase the durability of friction steel surfaces as well as parts subjected to abrasion wear.

Table 10. Experiment conditions in coating wear study

No.	Parameter	Value
1	Normal load	$P = 5$ N
2	Nominal contact area	$A = 2.25$ cm^2
3	Nominal contact pressure	$p = 2.22$ N/cm^2
4	Speed of rotation	$n = 212$ min^{-1}
5	Sliding speed	$V_c = 0.15$ m/s
6	Abrasive surface	Corund P320
7	Ambient temperature	$T° = 21°C$

Table 11. Parameters of wear of test samples at 200 friction cycles

No.	Pattern, electrode/designation, regime	Mass loss, mg	Wear rate, g/min	Intensity, mg/m	Wear resistance, m/mg
1	NW15B10T20/45 steel, $E_2 = 0.03$J,	8.7	9.1	20×10^{-2}	5
2	NW15T20/210cr12 hardened steel, $E_3 = 0.05$J	10.3	10.7	24.2×10^{-2}	4.13
3	NW15T20/45 steel, $E_3 = 0.05$J	12.6	13.1	29.6×10^{-2}	3.3
4	NW15T20/210cr12 hardened steel, Ee = 0.3J	5.1	5.3	12.0×10^{-2}	8.35
5	NW15B10T20/45 steel, $E_6 = 0.3$J	7.6	7.9	17.8×10^{-2}	5.62
6	NW15T20/45 steel, $E_6 = 0.3$J	7.5	7.8	17.6×10^{-2}	5.68
7	NW15B10T20/45 steel, $E_3 = 0.05$J	5	5.2	11.7×10^{-2}	8.87
8	NW15B10T20/45 steel, $E_5 = 0.16$J	6.9	7.17	16.1×10^{-2}	6.21
9	NW15B10T20/45 steel, $E_4 = 0.06$J	6.5	6.8	15.2×10^{-2}	6.56
10	NW15B10T20/210cr12 hardened steel, $E_6 = 0.3$J	6.5	6.8	15.3×10^{-2}	6.55
11	NW15B10T20/.45 steel, $I = 22$A, $C = 5$ μF, $T_i = 12$ μs, $n = 2$	6.5	6.8	15.3×10^{-2}	6.55
12	NW15B10T20/210cr12 steel, $I = 22$A, $C = 5$ μF, $T_i = 12$ μs, $n = 2$	5.6	6.8	13.1×10^{-2}	7.62
13	WK9/210cr12 steel, $I = 25$ A, Ti = 12 μs, $C = 5$ μF, $n = 2$, $E_2 = 0.03$J	8.5	8.9	19.9×10^{-2}	5.0
14	WK9/45 steel, $E_5 = 0.16$J	10.5	10.9	24.6×10^{-2}	4.06
15	P25/45 steel, $E_5 = 0.16$J	9.8	10.2	22.96×10^{-2}	4.35
16	WK9/45 steel, $E_3 = 0.05$J	14.8	15.4	34.6×10^{-2}	2.88
17	P25/45 steel, $E_5 = 0.16$J	11.2	11.6	26.2×10^{-2}	3.81
18	WK9/st210Cr12, $E_3 = 0.05$J	11.7	12.1	27.4×10^{-2}	3.65
19	P25/210cr12 steel, $E_5 = 0.16$J	8.9	9.2	20.8×10^{-2}	4.5
20	210cr12 hardened steel	19.7	20.6	46.1×10^{-2}	2.17
21	45 steel	29.3	30.68	68.7×10^{-2}	1.46

The pulse energy denoted by E_i refers to ESD with a vibrating electrode (Table 1). The regimes denoted with current I, capacitance C, and duration of pulses T_i refer to LESD.

As can be seen from Table 11 and Fig. 10, the effect of ESD differs according to different sliding distances. At the beginning of the work, both the differences in wear and the differences in the durability of the coated with different electrodes specimens are smaller. With increasing time and the sliding distance to 20−30 m, the effect of ESD increases to maximum peak values − to more than 6 times. With a further increase in the sliding distance, the coatings gradual is wiped, and, as a result, the effect is reduced monotonically by 2−5.5 times at a sliding distance 40 m, and then remains relatively constant. The highest values of the effect of ESD were observed in the second part of the curve of wear—after the initial smoothing of the friction surfaces.

When analysing the influence of the electrode materials on wear, it was found that the specimens of 45 steel coated with NW15B10T20 electrode at regimes with energy Ee = 0.05−0.06J have the lowest wear—to 1.2−1.5 times lowers than that of those

coated with WK9 electrode (Figure 10a,b). The lowest values of the wear of the samples coated with the new electrodes on 45 steel are close (Fig. 10b, Table 11), while the wear of those coated with NW15B10T10 electrode was up to 20% lower than that of those coated with NW15T20 electrode. Apparently, the combination of TiB_2, B_4C, and WC in the composition of the electrode allowed to use the full advantages of each of the individual component and to receive higher wear resistance of the layered surfaces compared to that obtained with only WC—TiB_2 or with WC-Co electrodes. The presence of B_4C in the electrode composition is the main reason for a higher wear resistance of these coatings. Super-hard B_4C has a dual role. The transferred particles firmly entrapped in the metal matrix of the coating increase its resistance to wear and, on the other hand, partial dissociation of B_4C in the transfer process serves as a B and C donor and promotes the formation of new borides and carbides (Tables 5, 6) which additionally contribute to an increase in the wear resistance of the coating.

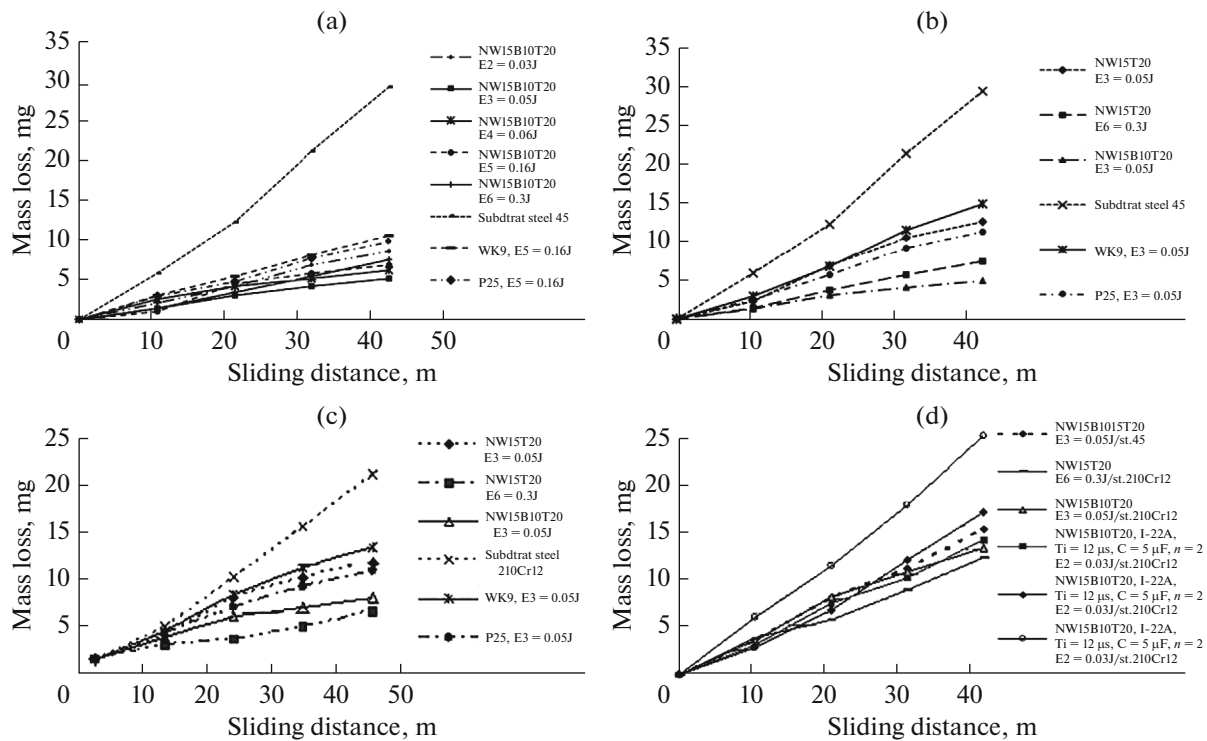However, for 210cr12 steel (Fig. 10c and Table 11), the lowest wear exhibited ESD samples with

Fig. 10. Mass loss vs. sliding distance of tested coatings: (a) NW15B10T20 electrode on 45 steel; (b) NW15T20 electrode on 45 steel; (c) on X12 steel: (d) obtained by ESD and LESD processes.

NW15T20 electrode in the regime at Ee = 0.3J—by about 20% lower than those at ESD with NW15B10T20 electrode and up to 50% lower than that of the coated specimens with WK9 and P25 electrodes.

The comparison of the wear of the coatings applied by vibration ESD and by LESD (Fig. 10d) shows that at the ESD with a vibration electrode, the wear of the specimens from both studied steels is lower. The differences, however, are not high: they reach only up to 10−15% at 200 load cycles. Still, at the beginning of the process, until the friction path passes to 20 m, the wear of the LESD samples is a little lower than that of vibration ESD. This is obviously due to lower roughness of LESD coatings. Subsequently, due to their lower thickness, these coatings are erased faster and their wear-resistance gradually decreases over time.

The obtained results show, that with new electrodes, coatings have higher wear resistance under friction and abrasive conditions than the substrate and those obtained with WC-Co electrodes, and they may be efficiently used to strengthen rapidly wearing parts of 210cr12 steel and for protection of steel parts from severe wear applications.

CONCLUSIONS

Carbide composite multiphase electrodes have been made based on mixtures of Cr-Ni-B-Si with WC, TiB_2, and B_4C in varying percentages. Applying ESD, dense coatings with low roughness, thickness to 90 μm, and wear resistance over five times higher than that of coatless surfaces can be obtained.

The influence of the energy parameters of both LESD and vibration ESD processes on the roughness, thickness, composition, structure, and abrasion wear of coatings obtained was investigated.

From the XRD and SEM data on the coatings, it is found that their phase composition on both steels studied here is enriched with more carbides and borides than at ESD with conventional carbide electrodes and is closer to composition of a high-speed steel, which implies a significant improvement of the performance properties of the layered surfaces.

Experimentally, the limit values of the energy and the duration of the pulses are determined by dense and even coatings with acceptable roughness obtained with new electrode materials. The conditions and processing parameters for ESD, at which the lowest wear of the coated steel has been obtained, have been determined.

The least wear is at the coatings from HW15B10T20 electrode on 45 steel and at HW15T20 electrode onto 210cr12 steel. The high abrasion resistance of the coatings is due to the presence of B_4C and of the combination of TiB_2 and WC in the multi-metal matrix Ni-Cr-B-Si and Co, which is the main reason for higher wear resistance of these coatings.

The resulting dependencies can be used to control and manage the basic parameters and the tribological properties of the molded wear-resistant coatings and to develop technologies for the lamination of specific details and articles.

REFERENCES

1. Samsonov, G.V., Verkhoturov, A.D., Bovkun, G.A., and Sychev, V.S., *Elektroiskrovoe legirovanie metallicheskikh poverkhnostei* (Electrospark Alloying of Metal Surfaces), Kiev: Naukova Dumka, 1976.

2. Gitlevich, A.E., Mikhailov, V.V., Parkanskii, N.Ya., and Revutskii, V.M., *Elektroiskrovoe legirovanie metallicheksikh poverkhnostei* (Electrospark Alloying of Metal Surfaces), Chisinau: Shtiintsa, 1985.

3. Safronov, I.I., Topala, P.A., and Gorbunov, A.S., *Elektroerozionnye protsessy na elektrodakh i mikrostrukturno-fazovyi sostav legirovannogo sloya* (Electroerosive Processes on Electrodes and Microstructural-Phase Composition of Alloyed Layer), Chisinau: Tekhnika Info, 2009.

4. Brown, E.A., Sheldon, G.L., and Bayoumi, A.E., *Wear*, 1990, vol. 138, nos. 1−2, pp. 137−151.

5. Johnson, R.N. and Sheldon, G.L., *J. Vac. Sci. Technol., A*, 1986, vol. 4, no. 6, pp. 2740−2746.

6. Antonov, B., US Patent 3832514, 1974. http://www.google.ch/patents/US3832514.

7. Antonov, B., Panayotov, S., and Lyutakov, O., US Patent 4226697, 1980. http://www.google.ch/patents/US4226697.

8. Penyashki, T.G. and Kostadinov, G.D., *Agric. Eng.*, 2013, nos. 4−6, pp. 48−55.

9. Gadalov, V.N., Romanenko, D.N., Goryakin, I.M., Kamyshnikov, Yu.P., et al., *Uprochnyayushchie Tekhnol. Pokrytiya*, 2008, no. 4, pp. 33−36.

10. Bovkun, G.A., Vladkova, Z.I., Molyar, V., Penyashki, T., et al., *Sov. Surf. Eng. Appl. Electrochem.*, 1988, no. 1, pp. 9−12.

11. Verkhoturov, A.D. and Nikolenko, S.V., *Uprochnyayushchie Tekhnol. Pokrytiya*, 2010, no. 2, pp. 13−22.

12. Verkhoturov, A.D., Podchernyaeva, I.A., Pryadko, L.F., and Egorov, F.F., *Elektrodnye materially dlya elektroiskrovogo legirovaniya* (Electrode Materials for Electrospark Alloying), Moscow: Nauka, 1988.

13. Nikolenko, V., Verkhoturov, A.D., and Syui, N.A., *Surf. Eng. Appl. Electrochem.*, 2015, vol. 51, no. 1, pp. 38−45.

14. Kudryashov, A.E., Potanin, A.Yu., Lebedev, D.N., et al., *Surf. Coat. Technol.*, 2016, vol. 285, pp. 278−288.

15. Penyashki, T., Kostadinov, G., Mortev, I., and Dimitrova, E., *Tribol. J. Bultrib*, 2016, no. 6, pp. 154−167.

16. Penyashki, T., Kostadinov, G., Mortev, I., and Dimitrova, E., *J. Balkan Tribol. Assoc.*, 2017, vol. 23, no. 1, pp. 69−81.

17. Mirkin, L.I., *Spravochnik po rentgenostrukturnomu analizu polikristallov* (Handbook on X-Ray Analysis of Polycrystals), Moscow: Fizmatlit, 1961.

18. Penyashki, T.G., *Tribol. J. Bultrib*, 2014, no. 4, pp. 159−169.

19. Khromov, V.N. and Kuznetsov, V.S., *Uprochnyayushchie Tekhnol. Pokrytiya*, 2010, no. 12, pp. 18−21.